

Topography and volume measurements of the optic nerve using *en-face* optical coherence tomography

John A. Rogers, Adrian Gh. Podoleanu, George M. Dobre, David A. Jackson
Applied Optics Group, School of Physical Sciences, University of Kent, Canterbury, CT2 7NR, UK
ap11@ukc.ac.uk

Fred W. Fitzke
Department of Visual Science, Institute of Ophthalmology, 11-32 Bath Street, London EC1V 9EL, UK
smgx510@ucl.ac.uk

Abstract: A special imaging instrument was developed which can acquire optical coherence tomography (OCT) *en-face* images from the eye fundus, and simultaneously a confocal image. Using this instrument we illustrate for the first time the application of *en-face* OCT imaging to produce topography and perform area and volume measurements of the optic nerve. The procedure is compared with the topography, area and volume measurements using a confocal scanning laser ophthalmoscope.

©2001 Optical Society of America

OCIS codes: (170.4500) Optical coherence tomography; (170.4470) Ophthalmology; (120.3890) Medical optics instrumentation

References and Links

1. R. H. Webb, G. W. Hughes and F. C. Delori., "Confocal scanning laser ophthalmoscope," *Applied Optics*, **26**, 1492-1499 (1987).
2. W. H. Woon, F. W. Fitzke, A. C. Bird and J. Marshall, "Confocal imaging of the fundus using a scanning laser ophthalmoscope," *British J. Ophthalmology*, **76**, 470-474, (1992).
3. A. E. Elsner, S. A. Burns, J. J. Weiter, and F. C. Delori, "Infrared imaging of sub-retinal structures in the human ocular fundus," *Vision Research*, **36**, 191-205 (1996).
4. B. R. Masters, "Three-dimensional confocal microscopy of the human optic nerve in vivo," *Opt. Express*, **3**, 356-359 (1998), <http://epubs.osa.org/oearchive/source/6295.htm>
5. Heidelberg Retina Tomograph, Operation Manual. (Heidelberg Engineering GmbH, Heidelberg, 1997).
6. A. W. Dreher, P. C. Tso and R. N. Weinreb, "Reproducibility of topographic measurements of the normal and glaucomatous optic nerve head with the laser tomographic scanner," *American J. Ophthalmology*, **111**, 221-229 (1994).
7. F. S. Mikelberg, C. M. Parfitt, N. V. Swindale, S. L. Graham, S. M. Drance and R. Gosine, "Ability of the Heidelberg Retina Tomograph to detect early glaucomatous visual field loss," *J. Glaucoma*, **4**, 242-247 (1995).
8. D. U. Bartsch, W.R. Freeman, "Axial intensity distribution analysis of the human retina with a confocal scanning laser tomograph," *Exp. Eye Res.*, **58**, 161-173 (1994).
9. K. U. Bartz-Schmidt, A. Sengersdorf, P. Esser, P. Walter, R-D. Hilgers and G. K. Kriegstein, "The cumulative normalised rim/disc area ratio curve," *Graefe's Arch Clin Exp. Ophthalmol.* **234** 227-231 (1996).
10. D. Huang, E.A. Swanson, C. P. Lin, J. S. Schuman, W. G. Stinson, W. Chang, M. R. Hee, T. Flotte, K. Gregory, C. A. Puliafito and J. G. Fujimoto, "Optical Coherence tomography," *Science* **254**, 1178-1181 (1991).
11. J. A. Izaat, M. R. Hee, G. M. Owen, E. A. Swanson and J. G. Fujimoto, "Optical coherence microscopy in scattering media," *Opt. Lett.*, **19**, 590-592 (1994).
12. C. Puliafito, *Optical coherence tomography of ocular diseases*, (Thorofare, NJ, SLACK Inc., 1996).
13. Data sheets of Humphrey Instruments, Optical Coherence Tomography, Humphrey Instruments, (2992 Alvarado St., San Leandro CA 94577, 1996).
14. J. S. Schuman, T. Pedut-Kloizman, E. Hertzmark, M. R. Hee, J. R. Walkins, J. G. Cooker, C. A. Puliafito, J. G. Fujimoto, E. A. Swanson, "Reproducibility of Nerve Fiber Layer Thickness Measurements Using Optical Coherence tomography," *Ophthalmology*, **103**, 1889-1898 (1996).

15. A. Gh. Podoleanu, M. Seeger, G. M. Dobre, D. J. Webb, D. A. Jackson and F. Fitzke "Transversal and longitudinal images from the retina of the living eye using low coherence reflectometry," *J. Biomed Optics*, **3**, 12-20 (1998).
16. A. Gh. Podoleanu and D. A. Jackson, "Noise Analysis of a combined optical coherence tomography and confocal scanning ophthalmoscope," *Appl. Opt.*, **38**, 2116-2127 (1999).
17. A. Gh. Podoleanu, J. A. Rogers, D. A. Jackson, S. Dunne, "Three dimensional OCT images from retina and skin," *Opt. Express*, **7**, 292-298, (2000), <http://www.opticsexpress.org/framestocv7n9.htm>
18. R. N. Weinreb, Lusk, D-U Bartsch and D. Morsman, "Effect of repetitive imaging on topographic measurements of the optic nerve head," *Arch Ophthalmol.*, **111**, 636-638 (1993).
19. W. Drexler, U. Morgner, R. K. Ghanta, F. X. Kartner, J. S. Schuman, J. G. Fujimoto, "Ultrahigh-resolution ophthalmic optical coherence tomography," *Nature Medicine*, **7**, 502-507, (2001).
20. D.S.Chauhan and J. Marshall, "The Interpretation of Optical Coherence Tomography Images of the Retina," *Investigative Ophthalmology*, **40**, 2332-2342 (1999).
21. C. K. Hitzenberger, A. Baumgartner, A. F. Fercher, "Dispersion induced multiple signal peak splitting in partial coherence interferometry," *Opt. Commun.*, **154**, 179-185, 1998.
22. R. H. Webb, "Scanning laser ophthalmoscope", in *Noninvasive diagnostic techniques in ophthalmology*, B. R. Masters ed, (Springer-Verlag, New York, 1990), pp. 438-450.
23. American National Standard for the Safe Use of Lasers: ANSI Z 136.1, (Laser Institute of America, New York, NY, 1993).
24. A. Gh.Podoleanu, J. A. Rogers, D. A. Jackson, "OCT *En-face* Images from the retina with adjustable depth resolution in real time," *IEEE Journal of Selected Topics in Quantum Electron.*, **5**, 1176-1184 (1999).
25. F. C. Delori and K. P. Pflibsen, "Spectral reflectance of the human ocular fundus," *Appl. Opt.*, **28**, 1061-1077 (1989),.
26. J. van de Kraats, T.T.J.M.Berendschot, D. van Norren, D, "The pathways of light measured in fundus reflectometry," *Vision Res.*, **35**, 2229-2247 (1996).
27. Elsner AE, Moraes L, Beausencourt E, et al., "Scanning laser reflectometry of retinal and subretinal tissues," *Opt. Express*, **6**, 243-250 (2000) <http://www.opticsexpress.org/oearchive/source/21766.htm>
28. A.E. Elsner, M. Miura, S.A. Burns, E. Beausencourt, C. Kunze, L.M. Kelley, J.P. Walker, G.L. Wing, P.A. Raskauskas, D.C. Fletcher, Q. Zhou and A.W. Dreher, "Multiply scattered light tomography and confocal imaging: detecting neovascularization in age-related macular degeneration," *Opt. Express*, **7**, 95-106 (2001) <http://www.opticsexpress.org/oearchive/source/22805.htm>
29. E. Beausencourt, A. E. Elsner, M. E. Hartnett, C. L. Trempe, "Quantitative analysis of macular holes with scanning laser tomography," *Ophthalmology*, **104**, 2018-2029 (1997).
30. C. Hudson, S. J. Charles, J. G. Flanagan, A. K. Brahma, G. S. Turner and D. McLeod, "Objective morphological assessment of macular hole surgery by scanning laser tomography," *British J. Ophthalmol.*, **81**, 107-116 (1997).

1. Introduction

Quantitative imaging of the optic nerve head in the living human eye is becoming increasingly important as a means of characterising its three dimensional structure with elevated intraocular pressure in glaucoma. Detecting abnormalities and change in the structure is important in finding damage and progression of damage. Among the challenges of characterising its structure are limitations in precision and accuracy of the measurements which are partly determined by the depth resolution of the imaging system. In addition the complex tissue structure with non-planar reflecting surfaces and semi-transparent overlying neural tissue makes it a difficult task.

High resolution imaging and tomographic assessments in the eye fundus are largely achieved using a confocal scanning laser ophthalmoscope¹ (CSLO). The influence of scattered light from outside the focus point within the target is suppressed by a pinhole in front of the photodetector and conjugate to the focal plane^{2,3}. 3D imaging⁴ is performed by acquiring *en-face* images at different positions of the focusing element, each position corresponding to a different depth. For instance, a CSLO such as the Heidelberg Retinal Tomograph (HRT)⁵ collects a stack of 32 *en-face* consecutive images at equidistant and different depths from within 0.5-4 mm depth in the retina. The HRT has also been developed to provide topography images⁶ and topographic parameters⁷ of the optic nerve by processing the stack of *en-face* images. For each pixel (x,y) in the transversal section, the reflectance intensity is determined as a function of scan depth⁸, z. The depth position of the peak in the axial intensity distribution versus depth is then used to build a topography map. As a quantitative imaging tool, CSLO can be used to provide 1D, 2D and 3D measurements⁷ such as: retina thickness, areas of the disk, cup, rim, the ratio of the cup and disk areas and volumes of the cup and the

rim, etc⁹. Computation and analysis of these parameters as well as topographic difference images are useful in the description of an optic nerve head, for glaucoma diagnosis and for the follow-up of the glaucomatous eye. Due to the intrinsic aberrations of the ocular components, the depth resolution^{2,5,8} of the CSLO is $\sim 300 \mu\text{m}$.

A method of higher resolution imaging of the retina is optical coherence tomography (OCT)¹⁰. In OCT, the depth exploration is obtained by scanning the optical path difference (OPD) between the object path and reference path in an interferometer illuminated by a low coherence source. Maximum interference signal is obtained for OPD=0. For an OPD larger than the coherence length of the source used, the interference signal diminishes considerably, which explains the selection in depth of the OCT¹¹. Generally, using superluminescent diodes, instrumental depth resolution better than $20 \mu\text{m}$ is achievable with OCT.

OCT has largely been applied to the fundus to create longitudinal images¹² (analogous to ultrasound B-scan) that are in-depth measurements through the retina. Practically, a B-scan image is constructed from many A-scans, which are reflectivity profiles versus depth (Figure 1). A commercial OCT instrument¹³ exists which can produce a longitudinal image of the retina in ~ 1 second.

However, using conventional longitudinal OCT, topography of the fundus is difficult to perform, unless many longitudinal images are collected for different *en-face* positions and orientations to cover a significant *en-face* area of the fundus. This may be performed in the same way as the retinal nerve fiber thickness is measured with OCT, by repeating a number of circular cuts around the nerve¹⁴. However, such a procedure as well as any other longitudinal OCT procedure is cumbersome as it requires interpolation in the *en-face* plane. Obviously, it is more natural to construct the topography (which refers to an *en-face* image) from collected *en-face* images. Therefore we looked into ways to overcome this drawback by building an OCT system capable of producing *en-face* images¹⁵ of the fundus. Using this new instrument, topography can be performed with the instrumental depth resolution of the OCT technology, which is much better than that achievable with a CSLO.

A demonstration of *en-face* OCT based topography, area and volume measurements is made on the eye of one of the authors (AP). The results are compared with those obtained using a state of the art HRT. This is only for illustration purposes to demonstrate the capability of our dual system and not to compare the accuracy of two different technologies (OCT and CSLO) nor of the accuracy of our instrument with that of a commercial instrument (HRT).

2. System

Unlike the usual application of OCT to the eye fundus, where a B-scan (x,z) or (y,z) is obtained from successive A-scans with slow scanning in a transversal direction¹⁰⁻¹⁴, we scan fast transversally to produce a C-scan image at constant depth (i.e. a reflectivity map in the x,y plane). This is similar to the procedure used in any CSLO, where the fast scanning is *en-face* and the depth scanning (focus change) is much slower (at the frame rate)¹⁹. The orientation of a C-scan relative to a B-scan slice is shown in Figure 1.

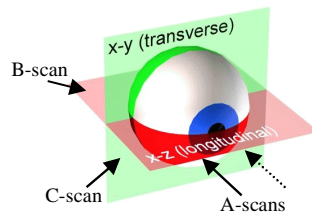


Fig. 1: Relative orientation of the axial scan (A-scan), longitudinal slice (B-scan) and *en-face* or transversal slice (C-scan).

at different depths¹⁷. Ideally, the depth interval between successive frames should be much smaller than the system resolution in depth and the depth change applied only after the entire C-scan image was collected. However, in practice, to speed up the acquisition, the translation stage was moved continuously. The movie in Figure 4 is constructed from a stack of 60 images collected while moving the stage at 40 $\mu\text{m/s}$. For the 2Hz frame rate this means 20 μm between the frames. In this way, 60 frame-pairs from a volume in depth of 1.18 mm in air are acquired in 30 s. In the movie in Fig. 4, only 50 frames were retained. The first 6 frames did not show any features and 4 other frames have been discarded due to blinks and movement effects.

The design is such that there is a strict pixel to pixel correspondence between the two *en-face* images (OCT and confocal). This helps in two respects: for small movements, the confocal image can be used to track the eye movements between frames and subsequently to transversally align the OCT images in relation to each other; for large movements and blinks, the confocal image gives a clear indication of the OCT frames which need to be eliminated altogether from the collection.

After the stack of pairs of OCT and confocal images has been collected, the confocal images are used to transversally align the pairs and hence the OCT images. Due to the alignment procedure, the transversal size of the images in the final set of aligned images is reduced from 300 x 300 to 210 x 210 pixels. As a reference for the aligning procedure, the first confocal image in the set is used.

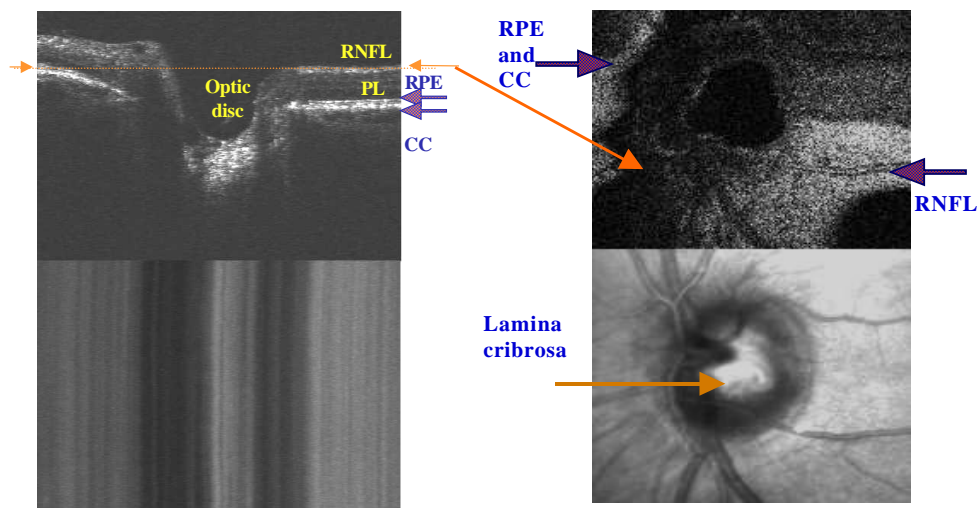


Fig. 3. Pair of images from the optic nerve acquired with the standalone OCT/confocal system in longitudinal regime at $y = 0$. Top image: OCT; Bottom: confocal; Each image has 300x300 pixels.

Horizontal: $\Delta x \sim 3$ mm in both images; Δz (only the OCT image) ~ 2 mm depth (vertical axis, measured in air). RNFL (bright): retinal nerve fiber layer; PL (dark): photoreceptor layer; RPE (bright): retinal pigment epithelium; CC (bright): choriocapillaris.

Fig. 4. (1 MB) Movie showing the pair of images from the optic nerve acquired with the standalone OCT/confocal system in transversal regime.

Top image: OCT; Bottom: confocal. Each image has 300x300 pixels.

Horizontal: $\Delta x \sim 3$ mm, Vertical: $\Delta y \sim 3$ mm in both images. The volume is explored from the retinal nerve fiber layer to the retinal pigment epithelium, along the optic axis. The OCT image displayed is at the depth shown by the double arrow in Figure 3 top.

3. Resolution and safety

Based on the confocal principle, the instrumental depth resolution of a CSLO is limited to a full width half-maximum $IDR_C = 300 \mu\text{m}$ (due to the combined limited aperture of the eye and aberrations^{2,5,8}). Therefore the accuracy in depth location of different scattering features and in measuring surface topography and volume is limited. However, interpolation procedures coupled with peak location software can lead to a much better reproducibility in the estimation of the peak position in depth. (Topographic reproducibility⁸ is the ability to determine the axial location of the centerline of the axial intensity distribution under the assumption of a single interface layer). For instance, the HRT instrument is quoted as giving a reproducibility^{5,18}, $R_C \sim 20 \mu\text{m}$. Considering the instrumental depth resolution this means an improvement factor $IF = IDR_C/R_C = 15$ achieved by software processing means, based on interpolation and peak finding algorithms.

In OCT, the depth resolution is governed by the spectral properties of the low coherence source, and theoretically, the full width half maximum of the depth sampling profile should be half of the coherence length of the source, which can easily be much smaller than the achievable depth resolution of a CSLO. Obviously, the same software procedures as used for the topography based CSLO can be used for an OCT implementation. Considering the recently reported¹⁹ instrumental depth resolution of OCT in measuring the retina thickness, $IDR_{OCT} = 3 \mu\text{m}$, and the same value for the improvement factor extended to the OCT case, $IF = IDR_{OCT}/R_{OCT}$, a depth reproducibility $R_{OCT} \sim 0.2 \mu\text{m}$ would seem achievable. This shows the tremendous potential of OCT in providing high depth resolution. However, improvement in the instrumental depth resolution of OCT does not necessarily attract the same improvement in the final resolution when measuring tissue, as pointed out by comparisons between OCT images and histology²⁰ and due to the inherent movements of the retina. Variations in the indices of refraction of the intermediate layers up to the depth of interest, from an average value considered in OCT measurement, along with polarization effects due to birefringence of the optic nerve justify discrepancies between OCT and histology. Therefore, micron resolutions in tissue, although attractive, have to be considered with caution.

To assess the resolution performances of our system, we used a mirror which was moved axially through the focus of the interface optics. The FWHM of the signal profile was $16 \mu\text{m}$ in the OCT channel and $\sim 0.9 \text{ mm}$ in the confocal channel. All the depth values are measured in air. Thickness in the retina can be found dividing the axial distances by the index of refraction¹⁹, $n \sim 1.36$. The depth resolution of the confocal channel can in principle be improved to 0.3 mm by using a high NA interface optics and a sufficiently small pinhole. However, as long as much better depth resolution is achievable in the OCT channel, a low depth resolution in the confocal channel, sufficient to eliminate the reflections from the cornea, is acceptable. This allows a sufficient good quality CSLO image to be generated based on a small percentage of the signal reflected by the retina with the majority of the signal remaining in the OCT channel.

For simplicity, in what follows we will approximate the OCT depth resolution as $20 \mu\text{m}$ (in air) throughout the depth range, although for superficial layers, this may be close to the instrumental depth resolution, of $16 \mu\text{m}$ (as measured in air), while for deeper layers, larger values are expected due to scattering and uncompensated dispersion in the OCT system²¹.

Due to an $1/e^2$ beam diameter to the eye of 2.5 mm , the transversal resolution is expected to be $\sim 15 \mu\text{m}$, the same in both channels as reported elsewhere when using either confocal⁸ instruments or OCT¹⁴. Using this value as an approximation for the lateral pixel size, we can evaluate the maximum exposure time, according to the same procedure presented in reference²². For a line of 3 mm covering the retina (as a minimum to scan the optic disk), this gives 200 pixels. Taking into account the line rate of 700 Hz and the frame rate of 2 Hz , investigation with $250 \mu\text{W}$ is allowed for many hours²³ at 850 nm . Seen from a different

perspective, the power in our system is 4 times less than the power used in the commercial OCT instrument¹³ which should allow 4 times longer exposure.

4. Method

4.1. A'-scans

When *en-face* OCT is used, equivalent A-scans can be built using a stack of *en-face* images

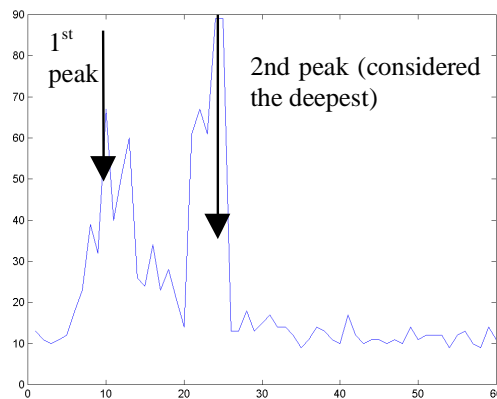


Fig. 5: Example of a software inferred A'-scan from the set in Figure 4, pixel 180x180, in a grid of pixels counted from the corner top left, up to 210 x 210 along X and Y axes. The continuous profile represents an interpolation over 60 points, one point for each OCT frame in the set, collected at a certain depth. Horizontal scale: Image number. Vertical scale: arbitrary units for the magnitude of the OCT signal. Interpolation was used to cover for the 4 frames removed from the collection.

collected at different depths. After the stack of images is aligned to eliminate the transversal movements between frames, a depth profile can be constructed for any (x,y) pixel by building the dependence of brightness versus the frame number. We will call such a depth profile, an A'-scan. In a similar way as CSLO is used for depth profiling⁸, individual software A'-scans are inferred from the stack of aligned OCT images. One such A'-scan is represented in Fig. 5. In opposition to the CSLO however, the sampling interval in our system can be smaller than the instrumental depth resolution. As another difference, troughs and pronounced minima are registered in the A'-scans for some depths positions where the reflectivity is low, as for example when collecting signal from the photoreceptor layer (PL). In CSLO, even when the depth is adjusted for the PL, the signal is high due to the larger depth profile than the retina thickness, which allows collection of back-reflected light from the high reflective fiber layer, retinal pigment epithelium and choriocapillaris.

For the example presented, the sampling interval was equal to the $IDR_{OCT} = 20 \mu\text{m}$. More frames can be collected at finer depth interval, with the consequence increase in the acquisition time. Compared with the HRT, the same depth range of 1.18 mm would be divided in 31 intervals, which gives $38 \mu\text{m}$ sampling interval.

4.2. Topography

Due to the multiple peak appearance A'-scans, a criterion is required for selecting the reflectivity peak that determines the depth position of the surface, the first peak, the highest peak, or the first peak with an amplitude above a certain threshold.

The very issue of building the height profile requires special procedures to cover the encountered discontinuities in the A'-scans. Such discontinuities arise due to the eye

movement, micro-saccades and due to the pulse that displaces tissue near the optic nerve head. The narrower the instrumental depth sampling interval, the more susceptible the topography method becomes to errors, due to movements or discontinuities in the reflectance profile.

For an image of 210x210 pixels there are 210^2 A'-scans to be evaluated. We reduced the number of samples by superposing A'-scans obtained from 6x6 adjacent transversal positions. This provided an averaging over both transversal and axial directions. Transversally, this results in an increase in the lateral pixel size while axially this leads to a smoothing of the A'-scans which provide an average A'-scan more tolerant to discontinuities due to artifacts. For comparison, the topography is provided by the HRT in a matrix of 16 x 16 elements. For an angular scan of 10^0 , the HRT element would have a size of $\sim 0.2 \text{ mm} \times 0.2 \text{ mm}$. 6 x 6 adjacent pixels leads to a matrix of 36 x 36 elements out of the area of 210 x 210 pixels of the aligned images in our case. This results in an element size of $60 \mu\text{m} \times 60 \mu\text{m}$. An optimum in the number of pixels to be averaged can be found only by imaging a large number of eyes. For the particular eye imaged here, 6 pixels seemed a good compromise between the required average and smoothing of the interpolation procedure and the deterioration of the transversal resolution.

Topography means in fact finding the depth position of a single layer surface. When the object is multi-layer, the problem is complex and a choice has to be made. Either the depth of the first scatterer or the depth of the scatterer with the highest backreflected signal is "sought" by the searching procedure. For this demonstration a simple thresholding method was applied. For too low a threshold, noise is collected while for too large a threshold, no peak may be detected. The optimum value of the threshold was adjusted until the position of the first peak in depth was consistent with the frame number in the collection, 1 to 60, which started to

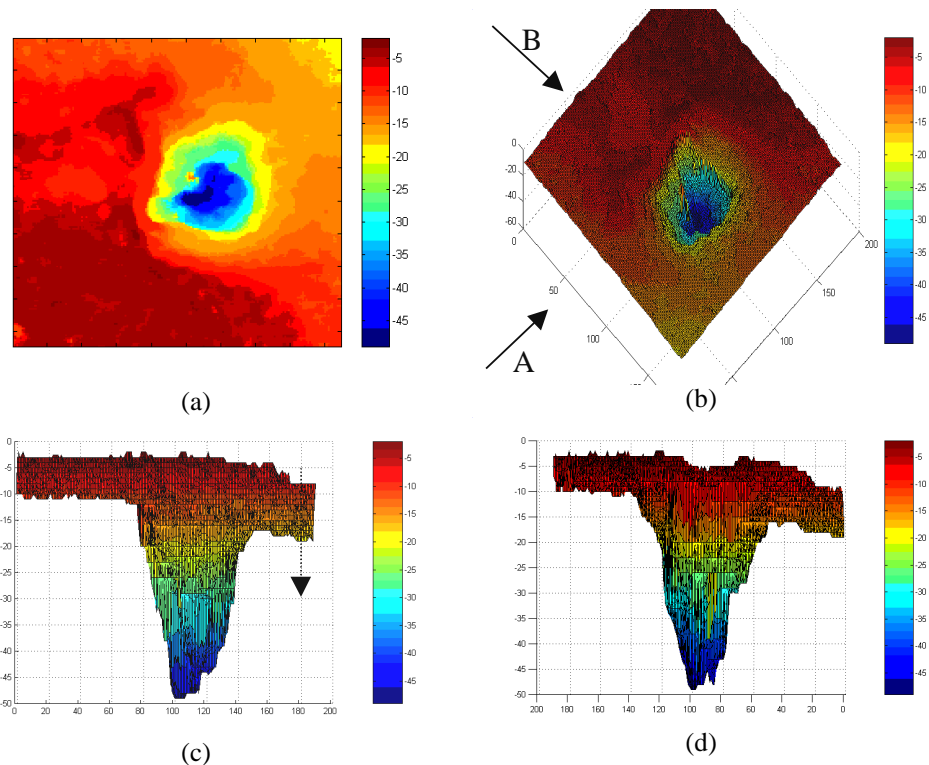


Fig. 6. Topography of the first surface, 186 x 186 pixels (1.9 mm x 1.9 mm). Depth map (values in color bar, the frame number, depth could be inferred by multiplying the frame number by 20 μm). (a):View from the top , along the z direction; (b): 3D view; (c): as seen from direction A in b; (d) as seen from direction B in b. The vertical arrow in (c) denotes the transversal position of the A'-scan in Fig. 5.

show a bright pixel. The topography of the first surface is represented in Fig. 6(a) and 3D views in Fig. 6(b-d). 14 more pixels have been removed from each side to avoid the edge effects, so the *en-face* image size is only 186 x 186 pixels.

It is also possible to produce a surface topography of deeper layers. This would be like effectively “looking” under the first surface “seeking” for features below the layer corresponding to the first peak. This can also be repeated for a third and so on, higher sequence peaks in depth.

To build the topography of the deepest layer, we searched for the first peak starting from the end of the A'-scans. We obtain similar representations as in Fig. 6 and represent both surfaces in Figure 7. Due to the high depth resolution of the OCT, the two surfaces are clearly discernible. We can approximate these two surfaces as corresponding to the retinal fiber layer and the choriocapillaris (please see Fig. 3 top, and Fig. 2 in reference¹⁹). The first peak in Fig. 5 contributes to the surface as shown by the arrow in Fig. 6c and to the top surface as shown by the arrow in Fig. 7c. The second peak in Fig. 5 contributes to the deepest surface as shown by the arrow in Fig. 7c.

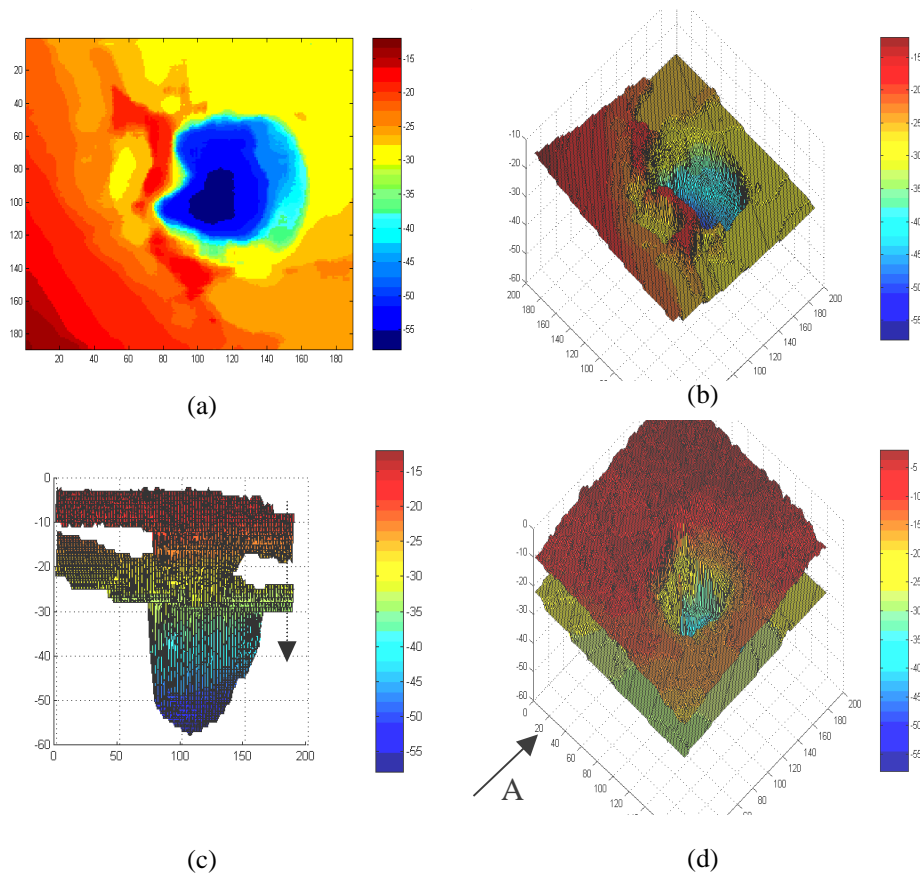


Fig. 7. Topography of the deepest surface, 186 x 186 pixels transversal (1.9 mm x 1.9 mm). Depth map (values in color bar, the frame number, depth could be inferred by multiplying the frame number by 20 μm ; the color map is different than that in Fig. 6.); (a): as seen from the top; (b): 3D view; (c): first and the deepest surfaces seen from the direction A in (d); (d): 3D views of the first and the deepest surfaces (Fig. 6(b) and 7(b) superposed).

4.3. Measurements:

For topography measurements of the optic nerve, a similar procedure to that performed by the HRT is employed^{5-7,9}. An arbitrary circle is drawn around the optic disk of the first image in the confocal set, as shown in Figure 8. The poorer depth resolution of our confocal channel, ~ 0.9 mm, in comparison with the depth resolution of the HRT, 0.3 mm, does not affect the analysis which follows, because we do not process the confocal images in depth. 180 A'-scans are collected for each point, (R, θ) positioned on the circle in Figure 8 at polar step angles θ of

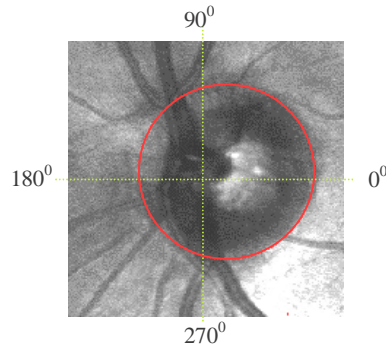


Fig. 8. The first image in the confocal set showing the contour line in red where A' scans are calculated (300 x 3000 pixels).

2°. Each A'-scan is made of $N = 60$ points.

Starting from points situated on the circle in Fig. 8, the depth position of the first significant peak in each A'-scan profiles is sought. Representing the depth position of such peaks on the polar angle θ , the depth variation in Fig. 9 is obtained. The profile is similar to the contour line variation height diagram produced by the HRT⁵.

For the demonstration of areas and volume measurements, the circle drawn on the confocal image in Figure 8 is taken to be the edge of the optic disk area. Estimating the original confocal image as of 3 mm by 3 mm, the optic disk area results as 2.63 mm^2 .

The HRT procedure^{5,7} relies on the definition of two planes, a reference plane and a surface plane. In our case, the surface plane of the retina is chosen at the depth of the frame 12 ($220 \mu\text{m}$), which corresponds to the mean height of the surface in Figure 9. The reference plane is chosen at 50 microns below the surface plane, following the HRT procedure^{5,7}. Two

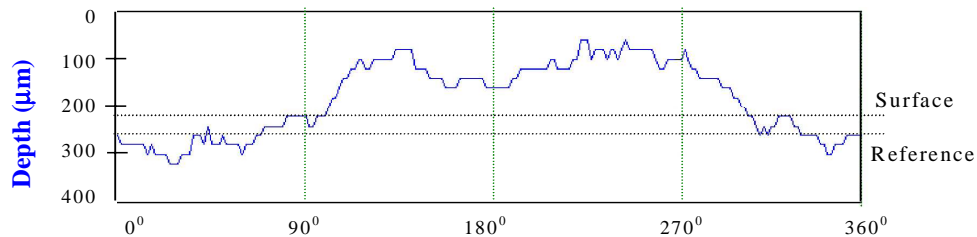


Fig. 9. Depth of the first surface, calculated from the depth position of the first peak in each A'-scan (such as that in Figure 5) originating on points situated on the contour drawn on the confocal image from the first frame in Fig. 8.

horizontal lines in Figure 9 show the depth position of the two surfaces. The area below the surface is called the effective area and the area below the reference plane is considered as the cup area. Volumes can be defined similarly, a list of these areas and volumes is presented in

reference⁷. It is hoped that these measurements can help an automated classification of the optic nerve shapes as belonging to the category of normal or glaucomatous eyes.

The results of the measurements are shown in Figure 10 left. The volunteer has had his eye assessed with the HRT. As far as possible the disk areas were adjusted to be the same. These areas are the starting point of the topographic measurements. Errors could not be totally avoided, as the two instruments are at different sites. Differences are noticed between the results obtained with the *en-face* OCT and with the HRT. A Cup/Disk area ratio of 0.44 results in comparison with the 0.329 value returned by the HRT. The value of other measurements in Fig. 10 can be compared with the HRT results presented in the Table 1.

4.4. Simulated Longer Resolution Lengths:

To eliminate the discontinuities in the A'-profiles, 6x6 pixels have been put together as mentioned before. It is possible to perform a similar averaging procedure in depth. This is equivalent to sampling the tissue in depth with a coarser depth resolution, in the same way as suggested by us in a previous publication where we discussed *en-face* OCT imaging with adjustable depth resolution²⁴. Depending on the number of frames from adjacent layers which are added together to produce one frame, the equivalent depth resolution is increased over the instrumental depth resolution, IDR_{OCT} . Such a procedure results in a smoothing of the A'-scans. In this way, we can "fabricate" a set of images with the instrumental depth resolution of the HRT and evaluate the effect on the measurements. To achieve this goal, we superposed each 15 adjacent OCT images in the set of aligned *en-face* OCT images to generate images with an equivalent of 300 μm sampling interval (this is an approximation, considering the resulting depth sampling interval as 15 x instrumental depth resolution approximated as 20 μm). The 300 μm value is specifically targeted as this is usually considered as the CSLO limit of depth resolution in the eye, and similar to that of the HRT. The results of measurements performed on the software fabricated set, are shown in Figure 10 right and Table 1. The result for the cup area is now smaller, closer to the value obtained with the HRT.

The depth resolution decreases with the number of adjacent *en-face* images which are

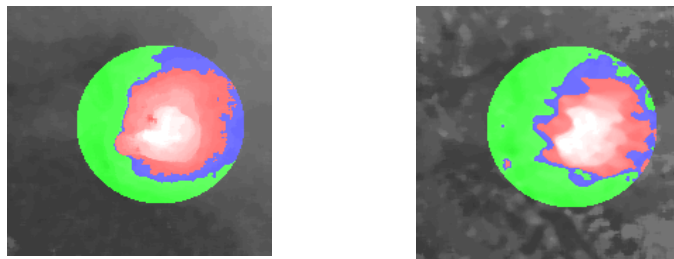


Fig. 10. Colored map topography of the first surface. The colored areas correspond to: green, the area above the surface, blue, the area between the surface and the reference plane and red the area below the reference plane. Values for areas are given in the Table 1.

Left: data were processed using the OCT depth resolution;

Right: data from the fabricated set of 300 μm depth resolution.

superposed. Therefore, further studies are necessary to find the optimum number of frames to be superposed, as a compromise between the ease in locating the peaks in the A'-scans and the error magnitude in area and volume measurements.

Differences are noticed between the quantitative measurements of the optic nerve taken with the commercial confocal retinal tomograph (HRT) and with our *en-face* OCT based retinal tomograph. Different sources of errors are possible. First, the two instruments are at two different sites and a perfect match of the areas imaged was not possible. Second, instrumental differences may play an important role. The different wavelength may be responsible for some of the differences observed, 675 nm (HRT) and 850 nm (OCT). Reflectivity and penetration depth of radiation of different wavelengths from visible up to

infrared was quantified in different reports, which show that longer wavelengths penetrate deeper^{3,25-27}. However, it is difficult to quantitatively assess, taking into account the complicated shape of the optic nerve, how the penetration depth influences the measurements. CSLO at longer wavelengths have been reported^{3,27,28}, however the authors are not aware of any comparative study of how the volumes and areas values measured with CSLO depend on wavelength.

Table 1. Comparative results for the areas and volumes in the optic nerve measured with *en-face* OCT and with HRT.

Parameter\System used	OCT 20 μm	OCT 300 μm	HRT 300 μm
Disk Area (user defined-whole disk)	2.63 mm^2	2.63 mm^2	2.607 mm^2
Effective Area (RED&BLUE)	1.613 mm^2	1.492 mm^2	1.462 mm^2
Rim Area (BLUE&GREEN)	1.63 mm^2	1.669 mm^2	1.748 mm^2
Cup Area (RED)	1.16 mm^2	0.949 mm^2	0.859 mm^2
Volume Below Reference (Cup Vol.-RED)	0.241 mm^3	0.234 mm^3	0.250 mm^3
Cup/Disk Area Ratio	0.44	0.36	0.329

It is interesting to notice that the coarser depth resolution set, obtained by putting together 15 adjacent *en-face* OCT images, provides measurement values closer to the HRT measurements. This may indicate that the depth resolution may play a role in explaining the differences noted. It is however too early to speculate based on only one eye investigated that coarser depth resolution results in smaller cup areas and larger rim areas. Given the importance of statistical relevant topography measurements for the follow-up of the glaucomatous eye, such a study may be worth pursuing on a large number of patients.

4.5. Utility of the confocal channel

To perform topography in the way illustrated in the paper, the confocal channel is not absolutely necessary. The topography was performed using the *en-face* OCT images. However, the dual representation unique for our system has helped in two respects:

(i) The relative movements of the confocal images is easier to track than the movements in the *en-face* OCT images. The OCT image may not show anything or be so fragmented that it cannot be processed. For instance, any alignment procedure would need to track relevant features in the stack of images. The chosen feature may or may not appear in the displayed image, depending on the retina inclination and the depth. This is in contrast to the confocal image, which looks more continuous even when largely out of focus.

(ii) The depth profile is evaluated along a contour drawn around the optic disk. This contour can be for instance drawn over an image resulting from the superposition of all the OCT images in the stack. Such an image would correspond to an image with a larger depth sampling interval, practically equal to the exploration interval. However, we believe that such a procedure would deprive the image of its transversal quality, and therefore, the confocal image is better suited for drawing the contour.

5. Conclusions

The paper demonstrates that the OCT technology, performed *en-face*, could be a potential candidate for topography as well as for area and volume measurements of the optic nerve. The paper presents for the first time such topography and measurements, obtained using *en-face* OCT. The *en-face* OCT addresses the incompatibility in the aspect of current CSLO and OCT technologies, images acquired with the two technologies could now be easily compared. The compatibility in aspect of the images produced by CSLO and *en-face* OCT allows the application of all procedures initially developed around CSLO technology to be extended to the *en-face* OCT technology. This paper is a first demonstration of such a possible extension. The same procedures developed for CSLO topography have been extended to the *en-face* OCT.

The *en-face* OCT imaging seems more suitable to perform topography than the longitudinal OCT imaging. If the object is a surface oriented perpendicular to the optic axis, the *en-face* OCT can provide the topography in one single frame, while longitudinal OCT requires interpolation of many A-scans. In practice however, the object is more complicated. The same single surface if oriented obliquely to the optic axis also requires interpolation of the points in the axial direction from *en-face* slice to the next *en-face* slice progressing in depth. The *en-face* OCT based topography provides continuous surfaces, rectangular to the optic axis and requires interpolation in depth. The longitudinal OCT based topography provides continuous profiles in depth and requires lateral interpolation. For the same data rate, sampling intervals and number of pixels the two methods may be very similar. However, the *en-face* OCT imaging may allow a quicker inference of the approximate topography profile. The approximate topography may be visible in the very process of frame acquisition (as seen in the movie in Figure 4), which is not possible to grasp when performing longitudinal OCT. In longitudinal OCT, all the volume data needs to be acquired and software processed before any surface with orientation rectangular to that of scanning direction could be generated.

The major source of measurement variation from successive examinations is patient realignment and instrument adjustment. The possibility of working *en-face* allowed us to realize how critical for the OCT images is the orientation of the eye, which may not be so obvious in longitudinal OCT. In the longitudinal OCT, when the retina surface is inclined, the final image shows layers oriented along diagonal directions deviating from horizontal (considering an x,z or an y,z image). The tilt has a different effect in the *en-face* OCT image, visible in the fragmentation and asymmetry of the *en-face* image. A horizontal tilt will lead to more fragments either left or right while vertical tilt will result in more fragments either up or down in the image. The vertical tilt (inclination in respect to axis y) is not visible in longitudinal OCT performed horizontally (i.e. in the x,z images) and the horizontal tilt (inclination in respect to axis x) is not visible in the longitudinal OCT performed vertically (i.e. in the y,z images). However, the *en-face* OCT shows the surface tilt in a single image. This can be noticed in the movie in figure 4. The transversal distribution of fragments indicate the tilt orientation directly. Longitudinal OCT performed at many radial orientations around the center of the image can show the spatial orientation of the retina surface, but this is obtained only after full collection of data is performed. This may require the investigation to be repeated if the tilt was too high and some of the slopes in the surface to be constructed could not be detected.

Due to the high depth resolution, OCT allows better differentiation of layers than CSLO and additionally, topography of deep layers. An illustration was presented in providing the topography of the choriocapilaris layer, along with the topography of the retinal nerve fibre layer. If topography of deep layers can be performed accurately and reproductively, new information can be provided to the ophthalmologist, in addition to the information currently collected using the CSLO technology. It is hoped that further refinements of the technique and software procedure may allow the standalone OCT/confocal system to be successfully applied to topography of the macula^{29,30}.

This paper describes measurements collected with the HRT and the *en-face* OCT instrument from only one eye. The intention was to demonstrate the viability of *en-face* OCT based topography and not to make a thorough statistical analysis of the measurements provided by *en-face* OCT nor to compare the reproducibility of OCT with that of CSLO. Large number of eyes need to be imaged to prove the validity of the method for diagnostic purposes. Such a study, if performed, may suggest new procedures for better area and volume measurements. For instance, the high depth resolution may allow a better definition of the reference plane or a complete change in the measurement strategy, where strong localised reflections can be used as reference (for instance the RPE or the choriocapilaris layer).

Acknowledgements

The authors acknowledge the support of the UK Engineering and Physical Sciences Research Council and of the Ophthalmic Technologies Inc. of Toronto, Canada.